International Biodeterioration & Biodegradation 174 (2022) 105464

Contents lists available at ScienceDirect

International Biodeterioration & Biodegradation

journal homepage: www.elsevier.com/locate/ibiod

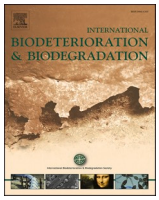

Hyperspectral imaging as a tool for profiling basidiomycete decay of *Pinus sylvestris* L.

Arnoud Jochemsen [a,*], Gry Alfredsen [b], Ingunn Burud [a]

[a] Norwegian University of Life Sciences, Faculty of Science and Technology, PO Box 5003, NO-1432, Ås, Norway
[b] Norwegian Institute of Bioeconomy Research, Division of Forestry and Forest Resources, Department of Wood Technology, PO Box 115, NO-1431, Ås, Norway

ARTICLE INFO

Keywords:
Fungal depolymerization
Basidiomycete fungi
Scots pine
Infrared
Hyperspectral imaging
PLS

ABSTRACT

Given the right climatic and environmental conditions, a range of microorganisms can deteriorate wood. Decay by basidiomycete fungi accounts for significant volumes of wood in service that need to be replaced. In this study, a short-wave infrared hyperspectral camera was used to explore the possibilities of using spectral imaging technology for the fast and non-destructive detection of fungal decay. The study encompassed different degradation stages of Scots pine sapwood (*Pinus sylvestris* L.) specimens inoculated with monocultures of either a brown rot fungus (*Rhodonia placenta* Fr.) or a white rot fungus (*Trametes versicolor* L.). The research questions were if the hyperspectral camera can profile fungal wood decay and whether it also can differentiate between decay mechanisms of brown rot and white rot decay. The data analysis employed Partial Least Squares (PLS) regression with the mass loss percentage as the response variable. For all models, the mass loss could be predicted from the wavelength range 1460–1600 nm, confirming the reduction in cellulose. A single PLS component could describe the mass loss to a high degree (90%). The distinction between decay by brown or white rot fungi was made based on spectral peaks around 1680 and 2240 nm, related to lignin.

1. Introduction

Wood is a common construction material, as it is light, strong, renewable, and available in abundance. However, as a natural material, wood is susceptible to biological deterioration. This deterioration takes place by fungi, insects, marine borers and bacteria. Basidiomycete decay fungi are the most efficient microorganisms that can decompose the wood (Zabel and Morrell, 2020). Decay fungi are typically subdivided into brown rot and white rot fungi (basidiomycetes) and soft rot (ascomycetes and fungi imperfection), although the delineation between brown rot and white rot is in reality more of a continuum (Riley et al., 2014; Zabel and Morrell, 2020).

Brown rot fungi mainly degrade conifers, while white rot fungi mainly degrade deciduous trees. The details of brown rot decay mechanisms, conditions for decay and enzymatic pathways are still under discussion, but it is generally agreed that brown-rot fungi use a two-step oxidative-enzymatic mechanism (Arantes and Goodell, 2014; Korripally et al., 2013; Wei et al., 2010; Zhang et al., 2016), and recent updates on brown rot decay mechanisms include e.g. (Castaño et al., 2018, 2021; Goodell et al., 2017; Presley et al., 2018, 2020; Presley and Schilling, 2017; Umezawa et al., 2020; Wu et al., 2018; Zelinka et al., 2021; Zhang et al., 2019a, 2019b, 2019c; Zhang and Schilling, 2017; Zhu et al., 2020).

Brown rot fungi degrade hemicellulose and cellulose while a modified (brown) lignin-rich residue is left behind (Kirk and Adler, 1970; Yelle et al., 2008, 2011). Brown rot fungi generally have greater effects on the elastomechanical properties of wood than white rot fungi (Winandy and Morrell, 1993). There are instances of brown rot fungi degrading significant portions of lignin such as *Gloeophyllum trabeum* (Adaskaveg et al., 1991; Schilling et al., 2012; Seifert, 1983), but complete lignin degradation is mainly known for white rot fungi. White rot fungi use powerful oxidative and hydrolytic enzymes that gradually degrade cellulose while lignin is completely mineralized, leaving lighter colored cellulose behind (Riley et al., 2014). White rot fungi can be divided into: 1. simultaneous/non-selective white rot – "removal of both cellulose and lignin, leaving cells either riddled with bore holes and erosion troughs, or with extensively thinned secondary walls" (Otjen and Blanchette, 1987) and 2. selective white rot – "lignin in the secondary wall and middle lamella is almost entirely removed, whereas large quantities of cellulose in the S2 layer of the cell wall are left intact" (Otjen and Blanchette, 1987).

There is a plethora of research on the application of near infrared

* Corresponding author.
E-mail address: arnoud.jochemsen@nmbu.no (A. Jochemsen).

https://doi.org/10.1016/j.ibiod.2022.105464
Received 4 March 2022; Received in revised form 11 July 2022; Accepted 13 July 2022
Available online 2 August 2022

(NIR) spectroscopy for the analysis of wood, and with good reason. NIR spectroscopy is a non-destructive measurement technique that requires little sample preparation and is sensitive to various wood characteristics. The absorption in the NIR wavelength range results from overtones and combination bands of the absorption peaks in the vibrational infrared and the signals are therefore much weaker and the penetration depth much larger (e.g. 1–4 mm vs 0.3 mm). In NIR spectroscopy there typically is a higher number of correlated variables (spectral bands) and a relatively low number of samples, and therefore multivariate data analysis is used.

A good overview of wood research with NIR spectroscopy is provided in the review papers of Tsuchikawa et al. (Tsuchikawa, 2007; Tsuchikawa and Schwanninger, 2013; Tsuchikawa and Kobori, 2015). Although NIR spectroscopy has been used for wood analysis for a couple of decades, the use of imaging spectroscopy or 'hyperspectral imaging' is a more recent development. Hyperspectral imaging captures a NIR spectrum for each pixel of an image, resulting in a spectral image.

For hyperspectral cameras in the NIR spectral range, one distinguishes between 'Visible and Near Infrared' (VNIR) and 'Short-Wave Infrared' (SWIR) cameras, because of a difference in detector technology: Silicon CCD for VNIR and InGaAs or MCT for SWIR. The SWIR range is approximately 1.0–2.5 μm and is as such a subset of the total NIR range (0.7–2.5 μm).

The applications of NIR hyperspectral imaging are for example detection of blue stain fungi on wood surfaces (Burud et al., 2014), classification of knots (Burud et al., 2015; Lestander et al., 2012; Sandak et al., 2020), quantification of weathering of wood (J. A. Sandak et al., 2016; Smeland et al., 2016), measurement of intra-ring wood density (Fernandes et al., 2013) and moisture content (Kobori et al., 2013; Stefansson et al., 2020).

A lot of NIR spectroscopy research into wood decay has been done by (Fackler et al., 2007; Fackler and Schwanninger, 2010, 2012; Kelley et al., 2002; Sandak et al., 2013; Schwanninger et al., 2004) and others. These research efforts in NIR spectral changes in decayed wood employ point spectrometry, typically using a Fourier-Transform Infrared (FTIR) instrument. In (Fackler and Schwanninger, 2012), an overview was given for 33 publications on fungal wood decay with spectroscopy, from 1967 until 2011. Nine of these were with *Pinus sylvestris* but not using NIR. Three reports were with diffuse reflectance NIR on *Picea abies*: two with FT-NIR and one with a dispersive spectrometer with a fiber optical probe (Kelley et al., 2002). In (Flæte and Haartveit, 2004), a NIR spectrometer with fiber optic probe was used on *Pinus sylvestris* inoculated with *Poria placenta* Fr. (current valid name is *Rhodonia placenta* Fr.) but the experimental results are listed solely as prediction errors while the spectral models are not described.

Previous studies have focused on NIR measurements of non-decayed or decayed wood using either a handheld point spectrometer on the specimens, a lab (Fourier-Transform) spectrometer on milled samples or a hyperspectral camera on non-decayed wood. The aim of this study was, for the first time, to evaluate if this type of hyperspectral camera could be used for fungal decay evaluation of solid wood surfaces. Using a hyperspectral camera to observe wood is nondestructive, unhindered by the heterogeneity of the wood, and allows for a spatial analysis of the fungal decay.

The research question is whether SWIR hyperspectral measurements can be used to characterize wood that has, to different degrees, been depolymerized by decay fungi and if it is possible to differentiate between brown rot and white rot decay i.e., two different wood depolymerization mechanisms.

2. Materials and methods

2.1. Preparation of the specimens

A total of 80 specimens of 20 × 20 mm and a thickness of 5 mm were cut out of a single board of Scots pine sapwood (*Pinus sylvestris* L.) originating from Indre Østfold municipality, Viken, Norway. The tree was harvested by the department of Wood Technology at NIBIO and was easily identified because there are only two species of forest forming conifers in Norway (Russell and Anderson, 2017). Scots pine has been used in this experiment because this wood species is one of the main commercial wood species in Northern Europe. The specimens were labeled and dried for 18 h at 103 °C, cooled down in a desiccator and dry weight was recorded with a Mettler Toledo ME303.

The specimens were climatized at 65% RH and 20 °C until they had reached a stable weight, which was at an average equilibrium moisture content (EMC) of 11.3%. Before inoculation, the media, the plastic meshes, and the specimens were all sterilized in an autoclave for 20 min at 121 °C. The Petri dishes were TC Dish 100, standard (Sarstedt AG & Co.), Ø = 87 mm, h = 20 mm. The malt agar medium contained 40 g malt from Difco and 20 g agar from VWR per 0.5 L of deionized water for the brown rot, and 40 g malt from VWR and 25 g agar from Dewert for the white rot. The reason for different media was to ensure optimal fungal growth conditions. A sterile plastic mesh (with a 1 cm hole in the middle for the inoculum) was added to each Petri dish to ensure that the wood samples were not experiencing any water logging. The inoculum was harvested from actively growing mycelia and a 4 mm plug was added, under sterile conditions, in the middle of the Petri dishes with the mycelia facing the media. Two wood specimens were exposed per Petri dish, after which the medium was either inoculated with *Rhodonia placenta* (Fr.) Niemelä, K.H. Larss. & Schigel, strain FPRL 280 – a brown rot fungus, or *Trametes versicolor* (L.) Lloyd, strain CTB 863 A – a simultaneous/non-selective white rot fungus, or not inoculated at all to maintain a reference specimen. These two fungi were chosen because they are frequently used model organisms. The two fungal species, and the same fungal strains, used in this experiment are e.g., specified in the European standards for testing of "Durability of wood and wood-based products. Test method against wood destroying basidiomycetes" (CEN 2020a,b). No parafilm was used to ensure sufficient ventilation.

The Petri dishes were put in a climate room at 70% RH and 22 °C, and five dishes (each containing two specimens) were harvested every other week, for 16 weeks, totaling 80 specimens. No contamination was found in any of the dishes. At each harvest the following samples were collected: two dishes with brown rot fungus; two dishes with white rot fungus; and one reference dish without a fungus. After harvest, the Petri dishes were immediately put in reusable zip-top bags and stored in a freezer at −32 °C. The reason for freezing the specimens was to be able to perform all end-of-experiment actions in a single session.

The Petri-dishes were taken out of the freezer and conditioned in a climate chamber at 70% RH and 22 °C for 4 h to get them to the same conditioned state as at the end of the incubation period in the climate room. The mycelium was gently removed with a scalpel, the specimens were dried for 18 h at 103 °C and weighed using the Mettler Toledo ME303. The dried specimens were stored in a desiccator and scanned with the hyperspectral camera.

The data resulting from the experiment are a set of specimen dry weights and a hyperspectral dataset. The initial dry weight at the start of the experiment ($W_{dry,start}$) and the final dry weight at the end of the experiment ($W_{dry,end}$) were used to calculate the mass loss percentage (ML) of the specimens:

$$ML = 100\frac{W_{dry,start} - W_{dry,end}}{W_{dry,start}}$$

The ML was used as the response variable in the data analysis because it indicates the change in weight and therefore the amount of decay that has taken place. Using this relative value eliminates the effect of the small differences in absolute weight between the specimens.

The hyperspectral datasets were recorded at the end of the experiment and consisted of one set of images of the front sides of the dried specimens, and one set of images of the back sides (facing the malt agar) of the dried specimens. Section 2.3 describes the datasets in more detail.

2.2. Hyperspectral measurement setup

The recording of the hyperspectral images was performed with the HySpex SWIR-384 from Norsk Elektro Optikk AS. This hyperspectral camera is a line scanner that records frames of 384 pixels by 288 bands over the spectral range 930–2516 nm. The lens of the camera had a 30 cm fixed focal length. The pixels had a size of approximately 0.25 mm, resulting in specimen images of about 80 × 80 pixels. The acquisition was carried out using the HySpex Ground v4.7.5 software and the conversion from raw data frames to radiances was performed using HySpex RADv2.

The specimens were transported under the line scanner by a translation stage. The specimens were lit using two semi-focused quartz tungsten halogen lamps from each side at an angle of ca. 70 °C. A Zenith Lite reference target from Sphere Optics (SG-3141-10-ALU) was located next to the specimens when they are scanned. See Fig. 1a for a sketch of the experiment setup and Fig. 1b for an example radiance image of a specimen.

2.3. Hyperspectral data pre-processing

The radiance (L) images (W nm^{-1} sr^{-1} m^{-2}) were converted to reflectance (R) by computing the average white reference value for each of the 384 pixels and 288 bands by:

$$R_{\Omega,B,sample} = R_{\Omega,B,reference}\frac{L_{\Omega,B,sample}}{L_{\Omega,B,reference}}$$

In which B is the spectral band and Ω is the solid angle that indicates the directionality of radiance from the pixel surface. $R_{\Omega,B,reference} \cong 95\%$ for all bands B. The pixels corresponding to the wood specimens were selected using simple object detection algorithms. The identification labels written on the front sides of the specimens were cut out and a three-pixel disc image erode was applied to the remaining image to remove any pixels that are not pure wood pixels. A reflectance image after object detection and image erode is shown in Fig. 1c. The images were converted from reflectance (R) to absorbance (A) using:

$$A = -\log_{10}(R)$$

The spectra of the hyperspectral pixels convey both chemical information and physical information of the material in the pixel area. The chemical characteristics are related to the vibrational energies of the molecules while the physical information is related to the surface and volumetric properties of the material. With the chemical composition of the material as our main interest, any path length variation due to physical effects was filtered out using Multiplicative Signal Correction (MSC). MSC assumes that the spectra have been affected by a wavelength-independent scaling and offset. The scaling and offset parameters are estimated from the sample spectra by regressing the spectra on a reference spectrum, which is often defined as the mean of all sample spectra (Geladi et al., 1985). Extended Multiplicative Signal Correction (EMSC) extends this two-parameter model by adding two additional wavelength dependent parameters and any known spectra (Martens et al., 2003; Martens and Stark, 1991).

The spectral bands at the extreme edges of the wavelength range are often left out prior to the analysis of hyperspectral pixels, because detectors typically exhibit noise in these bands (Ozaki et al., 2021). This study used the spectral bands in the interval from 1.0 to 2.5 μm. This meant the removal of the first nine and last three bands, resulting in spectra consisting of 276 spectral bands.

There are four absorption peaks of water within this spectral range, two strong peaks around 1430 nm and 1930 nm, and two very weak peaks that are both around 1180 nm (Ozaki et al., 2021). The water absorption around 1930 nm is about four times higher than it is around 1430 nm, and about hundred times higher than it is around 1180 nm. Because there are absorption peaks of cellulose and lignin around the same wavelengths (Schwanninger et al., 2011) and because the specimens were stored in a desiccator between drying and hyperspectral scanning, the effect of water on the spectra was assumed to be limited and all 276 spectral bands were included in the analyses of the spectra.

Two hyperspectral datasets were created from the recorded images (see Fig. S1). The first dataset consists of one spectrum and mass loss for each specimen and therefore consists of 80 spectra and 80 mass loss values. The second dataset consists of one spectrum for each image and therefore consists of 160 spectra, as there is one image for the front side of a specimen and one image for the back side of a specimen. The mass loss values of the specimens are repeated for both image spectra. The spectra and weights of the specimens were measured after the specimens have been dried (see section 2.1).

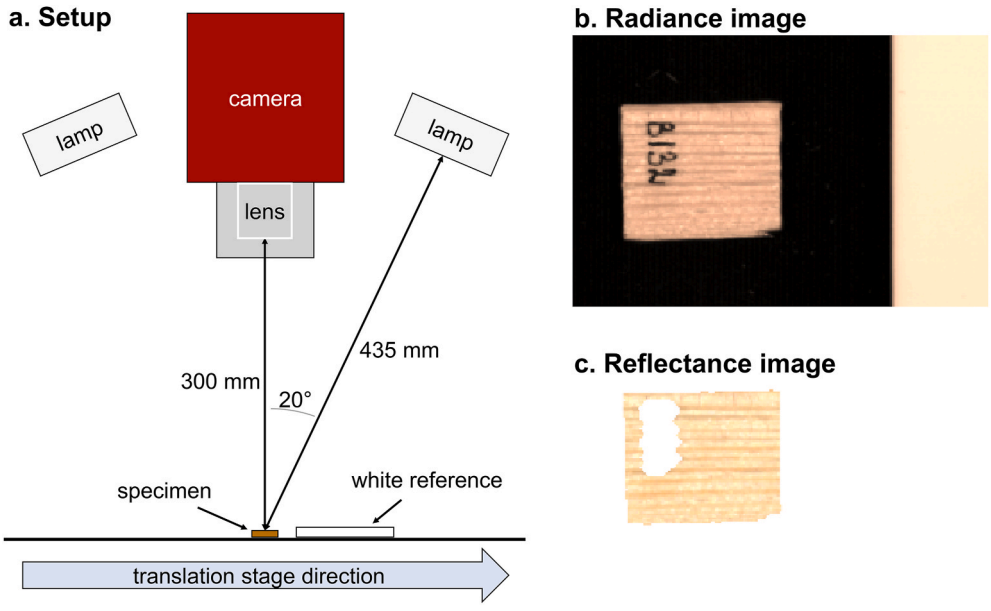

Fig. 1. a. Illustration of the experiment setup in which 20 × 20 × 5 mm wood specimens are scanned with a hyperspectral camera. b. Radiance image of the front side of a wood specimen in false RGB. c. Reflectance image of the same wood specimen shown in Fig 1b. The movement and lighting are in the direction of the wood fibers to minimize scattering effects and thereby minimize the number of saturated pixels.

2.4. PLS regression

Partial Least Squares regression (PLS) is a statistical method that finds a bilinear regression model by projecting both the independent and dependent variables to new vector spaces such that the covariance between the projected independent and dependent variables is maximized. Because the ML is a single dependent variable, the focus is on the analysis of the loadings of the independent variables.

The software used for the data analysis was Matlab R2021a, Mathworks. The PLS algorithm was the SIMPLS algorithm by (de Jong, 1993) as implemented in Matlab since 2008. The validation was full cross-validation (leave one out), and the number of components of the PLS model were selected manually based on explained variances. All data was used for the calibration and the cross-validation because the number of samples in the dataset was relatively low, and because the purpose of the PLS modelling was to explain the spectral changes of the wood due to the fungal decay.

2.5. Library spectra of wood chemical components

To aid in the explanation of the spectral changes due to fungal decay, library spectra of cellulose and lignin are visualized in Fig. 2. Cellulose and lignin are two most significant chemical components that make up Scots pine about 40.0% and 27.7% respectively (Sjöström, 1993). The NIR reflectance spectra of cellulose and lignin have been obtained from the Spectroscopy Laboratory of the United States Geological Survey (USGS), who has recorded the spectra with an ASD FieldSpec 3 HR (Kokaly et al., 2017). The reflectance spectra were converted to absorbance and MSC was applied to make the shapes of the spectra easier to compare.

Fig. 2a shows the mean spectrum of the reference specimens together with the two library spectra. The spectrum of cellulose closely resembles that of undecayed Scots pine wood. Fig. 2b shows the relative absorbances of the cellulose and lignin, which are obtained by subtraction with the reference spectrum. These relative differences can help explain the spectral changes in the wood specimens that have undergone fungal decay. For example: at 2485 nm, cellulose has a relatively higher absorbance than the wood. If the relative amount of cellulose decreases in a wood specimen, one would expect to see a relative decrease in absorbance around 2485 nm. Note that MSC was applied to the three spectra to better compare the shapes so it is relative changes in absorbance that are discussed.

Like all sensor acquisitions, these library spectra are affected by measurement errors to a certain degree. The lignin spectrum has a scattering artefact, and it seems to have a non-negligible moisture content (from the water peaks around 1430 and 1930 nm). Lignin varies between wood species as well as within wood species (Fernandes et al., 2013; Toivanen and Alén, 2006), and the lignin of the specimens is different from the lignin powder recorded by USGS. However, the various lignin polymers are still quite similar, and keeping any natural variation, contamination and measurement errors in mind, the library spectrum of lignin is still useful in the explanation of spectral changes of Scots pine sapwood due to fungal decay.

3. Results

3.1. Data exploration

Fig. S2 shows the ML due to fungal depolymerization over the duration of the experiment. The ML increased up to approximately 50% for a decay period of 16 weeks.

Fig. 3 shows the mean spectral absorbances for each of the groups of samples in the experiment: the reference specimen; the specimen decayed by the brown rot; and the specimen decayed by the white rot. There are clear differences in absorbances between the three groups of samples. The absorbances decrease when mass loss occurs (see Fig. 3a). The trend of decreasing absorbance for increasing decay is shown per fungi strain in Fig. S3. The trend of generally decreasing absorbance gets filtered out with MSC, which allows for an analysis of the relative change in the shapes of the average spectra (Fig. 3b).

3.2. Results for one spectrum per specimen

Fig. 4a shows a score plot of a two-component PLS regression model. The first component explains 32% of the variance in the spectra and 90% of the variance in the mass loss. The second component explains 57% of the variance in the spectra and only 2% of the variance in the mass loss. Together, these two components explain the variance in the spectra to a high degree ($32 + 57 = 89\%$). There are no influential outlier samples, i.e. samples with both a high residual and high leverage.

The two-component score-plot has the shape of an asymmetric and sideways V. The first PLS-component predominantly describes the spectral change due to the mass loss (for 90%). The higher the score for the first component, the more mass loss due to fungal decay. The second component describes the spectral differences between decay due to white rot and decay due to brown rot. The reference samples are in the center of component 2, the brown rot changes are negatively correlated to component 2 while the white rot changes are positively correlated.

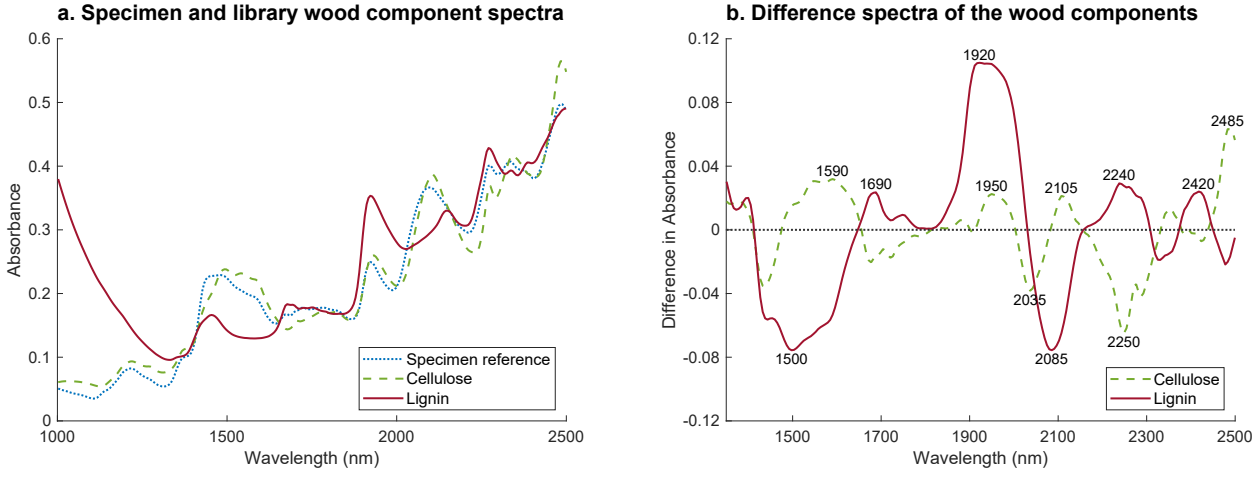

Fig. 2. Spectra of cellulose and lignin as in USGS Spectral Library Version 7 (Kokaly et al., 2017), as well as the spectrum of the reference specimens (no fungi). Figure a. shows the absorbance spectra with weighted MSC adjusted offset and scaling. Figure b. shows the relative absorbances of cellulose and lignin with respect to the reference specimens. The lignin has a scattering artefact for wavelengths shorter than 1350 nm so this wavelength range is not shown.

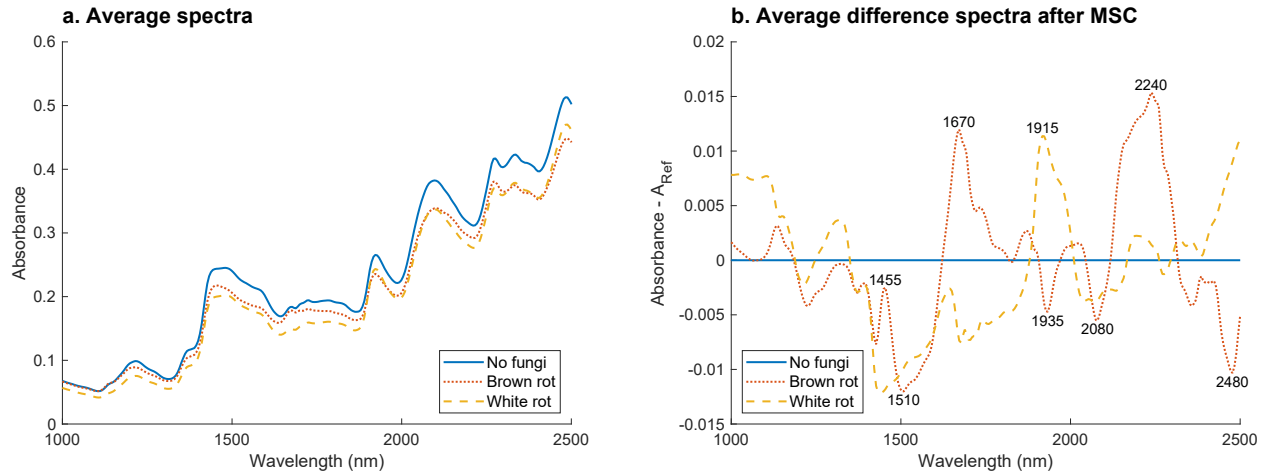

Fig. 3. The mean absorbances of the three groups of specimens: brown rot, white rot, and no fungi specimen. a. The average absorbances show a trend of decreasing absorbance with increasing decay. This is before the spectra are 'put on top of each other' by MSC. b. The absorbances after MSC, with the reference spectra subtracted, clearly show the differences in spectral change due to brown rot or white rot fungi.

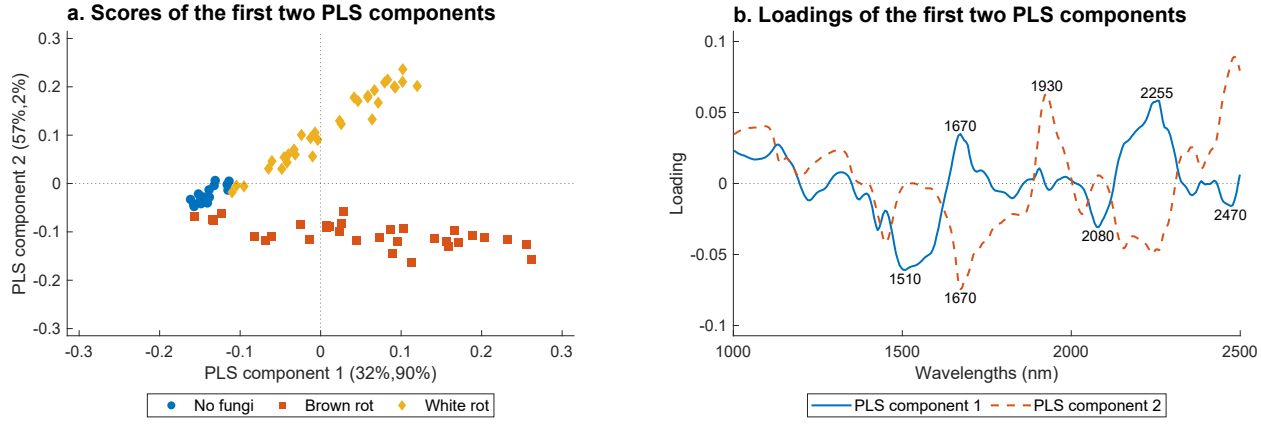

Fig. 4. Score plot (a.) and X-loading plot (b.) for the first two components of a PLS model that correlates the spectra of the specimens with their mass loss. The sample data represent 80 (spectra of) specimens, which have been dried after inoculation and incubation and consist of 32 samples with brown rot, 32 samples with white rot and 16 samples without inoculation.

Fig. 4b shows the loadings of the first two components. The loading of a component shows the importance of all variables for that component and reveal the spectral bands that are correlated to the mass loss (component 1), and the type of decay (component 2).

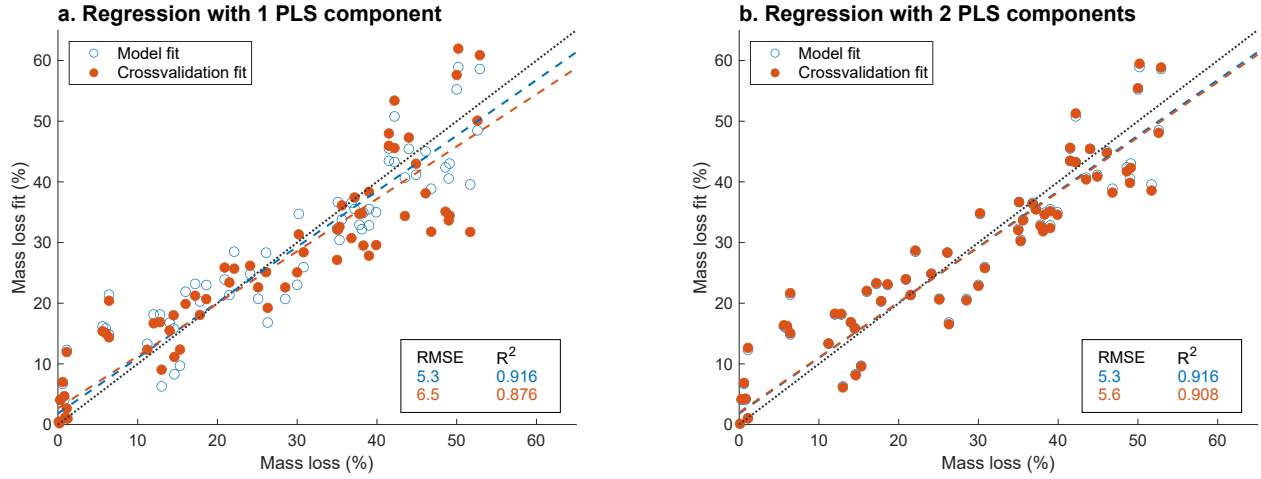

Fig. 5. Regression plot for a PLS model with just one component (a.) or two components (b.). The model fit has been created from all data, while the cross-validation fit models are created from leave-one-out cross-validation.

3.2.1. Regression plot

Fig. 5a shows the fit of the mass loss prediction when using a model with just a single component. The graph shows in general a good prediction of the mass loss from the wood spectra, with a Root Mean Square Error (RMSE) of 6.5% mass loss in cross-validation. Fig. 5b shows the regression results when both PLS components are used, which results in an RMSE of 5.6% in cross-validation.

3.3. Results for two spectra per specimen

When using separately the front image (facing up) and the back image (facing down) per specimen, the dataset consists of 160 samples (Fig. S1). Creating a PLS model with this dataset reveals the differences in decay of the front sides and the back sides (Fig. 6). For the white rot specimens, this difference is mostly in the first component, for which the front sides show a higher mass loss than the backsides. For the brown rot specimens, this difference is mostly in the second component, for which the front sides have a more pronounced brown rot decay spectrum. These effects can be more precisely analyzed by creating individual brown rot decay and white rot PLS models.

3.3.1. Model for the brown rot specimens

When making a model of just the brown rot specimens (32 specimens, 64 images), one can learn more about the difference in decay between the front sides and the back sides.

The first component in Fig. 7 represents the mass loss for about 80%, while the second component describes the mass loss for just 7% and mostly describes the differences between the front sides and back sides of the specimens.

3.3.2. Model for the white rot specimens

Making a PLS model using only the white rot specimens reveals better how the white rot fungus depolymerizes the wood. In Fig. 8, a PLS model for white rot with two components is visualized. The first component explains most of the mass loss (94%), while the second component again explains the differences between the front and the back sides of the specimens (and mass loss for only 1%).

3.3.3. Spatial distribution of the fungal decay

By multiplying the pixels of a hyperspectral image with the regression coefficients of a PLS model, it is possible to show a mass loss prediction for each pixel of the image. This allows for visualization of the spatial aspects of the fungal decay. Fig. S4 shows the predicted mass loss per pixel for the front and the back sides of specimen B132, which was also shown in Fig. 1.

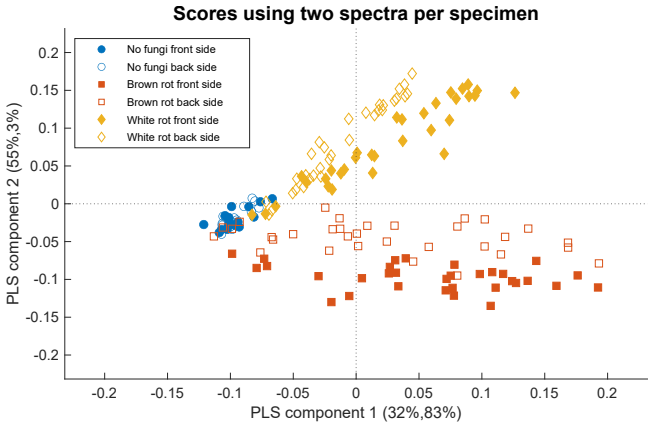

Fig. 6. Scores plot for the first two components of the PLS model based on two spectra per specimen, i.e. one spectrum for the front side and one spectrum for the back side. The loadings are identical to those of the model with one sample per specimen (Fig. 4b) and are not shown here.

4. Discussion

4.1. Data exploration

Fig. 3 and Fig. S3 show a trend of decreasing absorbance for increasing decay. This trend is similar to the results of another diffuse reflection spectroscopy study (Kelley et al., 2002). The apparent absorbance decreases due to the decrease in wood density as the wood decays. Less dense wood results in a lower absorbance, like earlywood showing less absorbance than latewood (i.e. earlywood looks lighter than latewood in the short-wave infrared). The Beer-Lambert law dictates that for similar pathlengths, a lower density leads to a lower concentration and thus lower absorbance. Another effect is that the decrease in wood density leads to a greater surface roughness, which for the setup as in Fig. 1, leads to more light scattering in the direction of the camera and thus a higher reflectance.

4.2. PLS results for one image per specimen

4.2.1. Scores

The PLS scores in Fig. 4 resemble a sideways and asymmetric V shape because the components of a PLS model are created such that they maximize the correlation with the response variable. In contrast to PLS, a principal component analysis (PCA) of the data leads to a score plot shaped like a symmetric and non-sideways V, because in a PCA, the components are created such that the variance of the projected data is maximized (PCA results not shown). In (J. Sandak et al., 2016) figure 5, a PCA is shown for the infrared spectra of spruce wood decayed by brown rot, white rot and no fungi. In their data analysis, the decay is for a single harvest point, and the three groups do not overlap at all. The third component of the PCA mostly defines the difference between non-decayed and decayed specimens and can be interpreted to represent the mass loss, which is represented by the first component of the PLS.

The scores of component 2 become more extreme as the decay time increases, for white rot more so than for brown rot. This asymmetry occurs because component 1 (mass loss) predominantly describes the spectral change of brown rot decay (see Figs. 4b and 7b), and component 2 describes the difference of the white rot spectral change relative to the brown rot spectral change. The PLS uses the brown rot decay spectral characteristic to model mass loss because the brown rot samples are more influential. This is because the brown rot changes the shape of the wood spectrum more than the white rot does, because brown rot is more selective in the depolymerization of the wood cell wall polymers (Rowell, 2005; Zabel and Morrell, 2020).

4.2.2. Loadings

The spectral range 1460–1600 nm is key in defining the spectral change due to mass loss. This spectral range is heavily linked to cellulose in literature (Schwanninger et al., 2011) and this can also be observed from the cellulose spectrum in Fig. 2. Because cellulose has much absorbance in this range, it leads to relatively less absorbance in this spectral range as the cellulose disappears when the decay fungi break it down. This can be seen in the loadings of component 1, which are negative for these spectral bands. Simply put: Increasing mass loss due to basidiomycete decay means more of component 1, which means less absorbance for ‘cellulose bands’ and therefore less cellulose.

The bigger spectral peaks around 1680 and 2265 nm are related to lignin (Fig. 2) (Schwanninger et al., 2011). For brown rot, the relative amount of lignin increases as the cellulose disappears, which leads to positive loading values for these peaks in component 1. PLS component 2 shows an inverse for the lignin peaks (Fig. 4). This shows a difference between the brown rot and the white rot decay fungi, which can be explained by the fact that white rot breaks down lignin, while brown rot does not. Less lignin leads to less relative absorbance for lignin wavelengths, and thus a higher score of component 2, which means a more ‘simultaneous white-rot’ spectral characteristic.

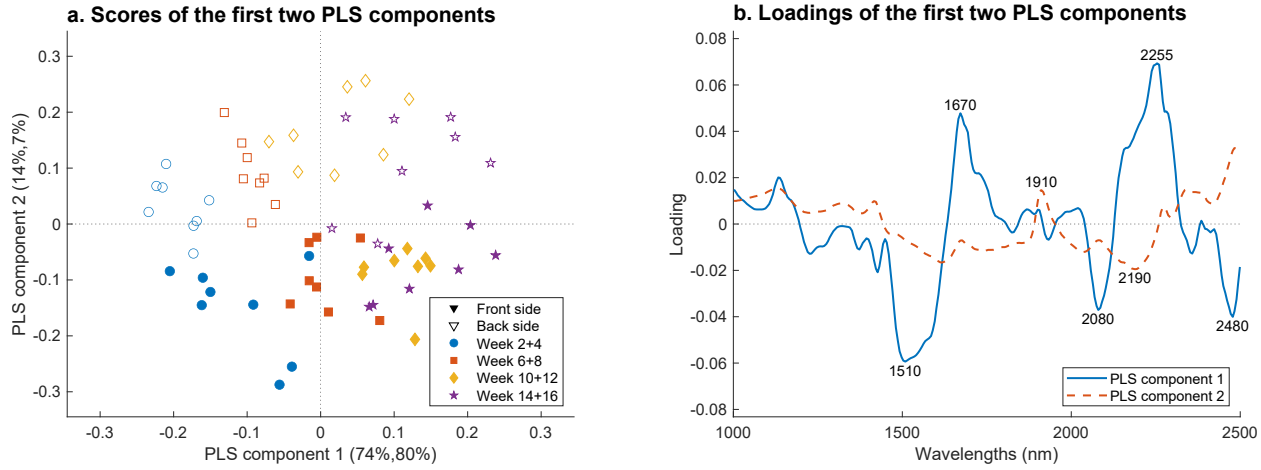

Fig. 7. Score plot (a.) and X-loading plot (b.) for the first two components of a PLS-model that correlates the spectra of the specimen with their relative mass loss. The sample data is the spectra of 32 specimens, which have been dried after incubation with brown rot fungus. Two spectra were recorded for each specimen, one from the front side and one from the back side.

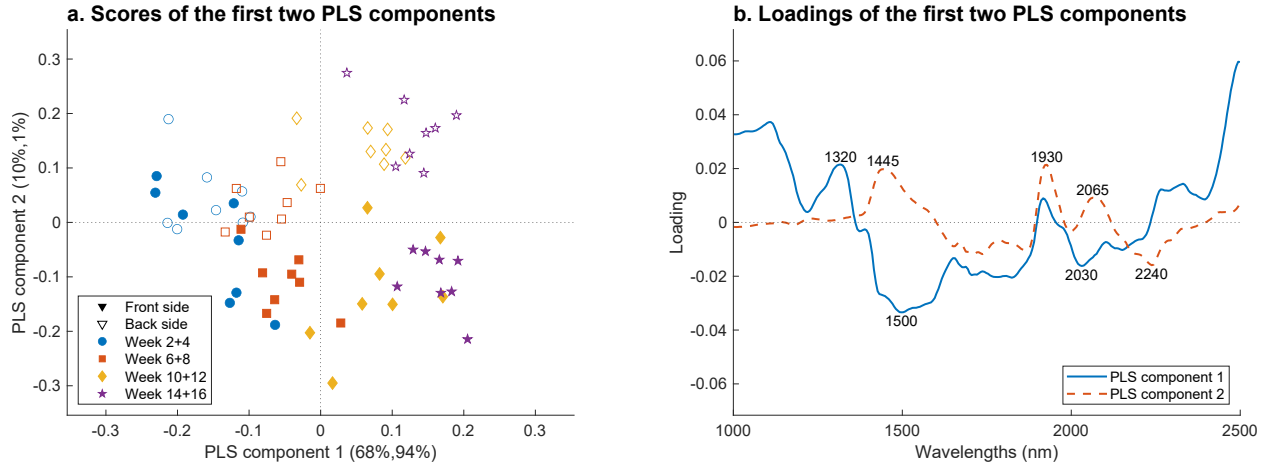

Fig. 8. Score plot (a.) and X-loading plot (b.) for the first two components of a PLS-model that correlates the spectra of the specimen with their relative mass loss. The sample data is the spectra of 32 specimens, which have been dried after incubation with white rot fungus. Two spectra were recorded for each specimen, one from the front side and one from the back side.

The USGS lignin library spectrum (Fig. 2a) shows the smaller lignin spectral peaks at 1726, 1791, 2140, 2336, 2385, 2489 nm (peaks not marked in Fig. 2a) that are also listed in the band assignments review (Schwanninger et al., 2011), which gives confidence in the interpretation of spectral changes observed around 1680 and 2265 nm.

4.2.3. The effect of water

Even though the specimens are kept in a desiccator between drying and hyperspectral scanning, it seems that the humidity was not controlled well enough to eliminate the effect of water entirely from the extremely hygroscopic dried wood specimens. In fact, even the relatively low moisture content of the specimens has a quite large effect on the measured spectra, because the absorbance of water in the short-wave infrared is so strong.

In the loadings plot in Fig. 4, a large peak is observed around 1930 nm for the loading of component 2, which differentiates brown rot and white rot decayed wood. Absorbance around 1930 nm is very strongly related to the O–H bonds of water, and to a lesser degree to the O–H in the lignin and cellulose (Curran, 1989). Note that in the milled lignin spectrum, this 'water band' is shown at 1920 nm in Fig. 2 (Kelley et al., 2002; Schwanninger et al., 2011).

The positive peak in the loading suggests that white rot decayed wood tends to hold more water and that the water content in the dried specimens increases with progressing white rot decay. This may happen because the dried white rot decayed specimens have a lower density than the other dried specimens, and because carbohydrates, such as (hemi)cellulose, are better at binding water than lignin (Rowell, 2005). The assessment of the specimen sizes from the hyperspectral images (Fig. S2) shows that the white rot specimens are approximately equal in size for all harvests, while the brown rot specimens shrink by up to 10% due to a difference in the decay mechanisms (Winandy and Morrell, 1993). With the mass loss approximately the same, the white rot specimens have therefore a lower density than the brown rot specimens. Note that the density calculation is based on the number of hyperspectral image pixels and is a rough volume estimation that is only based on the length and width of the specimens and not the thickness of the specimens.

The third component of the PLS model (not depicted) predominantly describes the water content. The amount of third component is seemingly randomly distributed among the samples. This means that despite the attempt at humidity control, the humidity leads to a relatively large variation in the spectra. In order to use more than two PLS components for more accurate prediction of decay, the effect of water on the spectra should be filtered out. This can be achieved by, for example, variable

selection (e.g. removing or down-weighing the water bands), or by more advanced pre-processing (e.g. EMSC).

4.3. Brown rot model

The loading of the first component is nearly identical to that of the complete model: more absorbance in the cellulose range 1460–1600 nm, and a higher relative presence of lignin, visible around 1670 nm and 2255 nm. (Figs. 4b and 7b).

The second component is of course quite different, because for the brown rot model it describes the differences between the front sides and the back sides of the specimens. The second component has small peaks corresponding to water (1430 and 1930 nm), which could indicate that the back sides of the specimens contain relatively more water than the front sides. Note that for the brown model, the first component accounts for 80% of the variance in the mass loss, which is lower than for the other models. Brown rot has a bigger difference between front sides and back sides, and while the front sides have a higher predicted mass loss up to week 10, the back sides have a higher predicted mass loss from week 12. This non-linearity can also be seen in the regression plot of Fig. 5, where the predictions become a bit less accurate for mass losses higher than 35%.

Fig. S4 shows the spatial distribution of the fungal decay for a brown rot inoculated specimen of week 16. The mass loss of the specimen is 53%, while the predicted mass loss is approx. 54%. The predicted mass loss from just the front side is about 2% lower, while the predicted mass loss for the back side is about 2% higher. The predicted amount of decay is not uniformly spread over the front and the back sides of the specimen, and it is not uniformly spread over the surfaces either. Earlywood and latewood are a factor in distribution of the mass loss over the specimen, as well as the edges of the specimens. The image shows that the decay of the back side was faster for this specimen, and that the decay is more in the center of the specimen, compared to the decay of the front side.

Another diffuse reflectance study reports a fairly strong negative correlation of the 1480, 1920 and 2090 nm peaks with the mass loss due to brown rot in spruce, i.e. a lower absorbance for a higher mass loss (Kelley et al., 2002). Similarities are the use of a two component PLS regression model, and strong negative correlation around 1480 and 2090 nm, shown at 1510 and 2080 nm. A notable difference in the results is for 1920 nm. This is probably due to the presence of water in this experiment, which then compensates for reduction of absorbance due to carbohydrate vibrations. Note that although (Kelley et al., 2002) likely had better humidity control, there are numerous other differences between the studies that could partially account for the difference in results, such as wood species, specimen size and spectroscopic instrument.

4.4. White rot model

The white rot model is quite different from the two other models, because the PLS model that used all samples was dominated by the spectral changes due to the selective depolymerization of polymers by the brown rot fungus. In contrast, the white rot fungus is non-selective and depolymerizes all the wood components.

The first component in Fig. 8b also shows the loss of absorbance around 1500 nm due to the loss of cellulose. This is the major similarity between the brown rot and white rot models and the main correlate for the mass loss when calibrating a model using all samples.

At 2500 nm, the first component shows an increase in absorbance for increasing mass loss, even though this wavelength was also associated with cellulose absorbance. This may be because the amount of water seems to increase, which may be seen in the peaks around 1440 nm and 1930 nm. Water also has a strong absorbance for 2500 nm, and this may offset the loss of absorbance due to the decrease in cellulose.

The second component shows the differences between the front sides and the back sides. This component largely seems to consist of a bit more cellulose, a bit less lignin and a bit more water.

Note that after only two weeks of decay, there is hardly any spectral difference between front side and back sides of the white rot specimens. The mass loss at this point is almost 0%. For the brown rot, however, there was already quite a spectral difference after two weeks even though the mass loss for those specimens was also around 0% after two weeks. The change in spectra, even without mass loss, is due to the faster depolymerization by the brown rot (Witomski et al., 2016).

4.5. Suggestions for further studies

Even though the dried specimens were stored in a desiccator, the water content of the specimens plays a key role in the spectral analysis of the changes in the wood. It is critical to estimate the water content from the spectra to enable reliable prediction of mass loss due to fungal decay from spectral images. In addition to the water content, the lignin and cellulose content could be estimated from the spectra. The prediction of these values would provide additional insights in the wood composition.

In this study, the physical effects such as light scattering were partly removed by MSC, which removes offset and scaling effects from the spectra. Better identification and elimination of the physical effects would require wavelength-dependent approaches. In addition, the estimation of the physical properties of the specimens might be just as valuable as the estimation of the chemical properties for the prediction of the condition of the decaying wood.

The average spectra of the images were used as input to the models in this study, which reduces the input data to the modelling by a few orders. More advanced processing could exploit the images to an extent beyond the front and back sides of the specimens and reveal the spatial aspects of progressing fungal decay with considerably more detail.

PLS models with two components were chosen for the modelling. A coarse interpretation of the meaning of the first loading components was relatively easy and due to the third component being mostly water related, a two-component model was found to be the most robust. A more common method to determine optimal number of model components is by cross-validation, which can find additional relevant patterns that are not found by human interpretation of the loadings.

Datasets 1 and 2 (Fig. S1) are available on Mendeley Data (Jochemsen, 2022).

5. Conclusions

It was found that the mass loss could be predicted from the SWIR spectra, i.e. a SWIR hyperspectral camera is suitable for quantification of basidiomycete decay. A single component PLS model was sufficient to capture 90% of the mass loss from the spectral change. Adding a second model component improves the cross-validation results and provides information on whether the mass loss was due to brown rot or white rot.

Declaration of competing interest

The authors declare the following financial interests/personal relationships which may be considered as potential competing interests:

Gry Alfredsen reports financial support was provided by Research Council of Norway.

Acknowledgements

Thanks to Thor-Erik Alstad (NIBIO) for making the samples and Sigrun Kolstad (NIBIO) for helping with the decay test.

This work is supported by the project RIWUP, which is led by NORCE and runs under Research Council of Norway (RCN) grant agreement nr 281018 and is co-funded by both RCN and Nettpartner. Part of the work was funded by the CLICK*design* project (RCN 297899), supported under the umbrella of ERA-NET Cofund ForestValue.

Appendix A. Supplementary data

Supplementary data to this article can be found online at https://doi.org/10.1016/j.ibiod.2022.105464.

References

Adaskaveg, J.E., Blanchette, R.A., Gilbertson, R.L., 1991. Decay. Of date palm wood by white-rot and brown-rot fungi. Can. J. Bot. 69, 615–629. https://doi.org/10.1139/b91-083.

Arantes, V., Goodell, B., 2014. Current understanding of Brown-rot fungal biodegradation mechanisms: a review. In: Schultz, T.P., Goodell, B., Nicholas, D.D. (Eds.), ACS Symposium Series. American Chemical Society, Washington, DC, pp. 3–21.

Burud, I., Gobakken, L.R., Flø, A., Kvaal, K., Thiis, T.K., 2014. Hyperspectral imaging of blue stain fungi on coated and uncoated wooden surfaces. Int. Biodeterior. Biodegrad. 88, 37–43. https://doi.org/10.1016/j.ibiod.2013.12.002.

Burud, I., Gobakken, L.R., Flø, A., Thiis, T.K., Kvaal, K., 2015. Hyperspectral near infrared imaging of wooden surfaces performed outdoors and indoors. NIR News 26, 4–7. https://doi.org/10.1255/nirn.1500.

Castaño, J., Zhang, J., Zhou, M., Tsai, C.-F., Lee, J.Y., Nicora, C., Schilling, J., 2021. A fungal secretome adapted for stress enabled a radical wood decay mechanism. mBio 12. https://doi.org/10.1128/mBio.02040-21 e02040-21.

Castaño, J.D., Zhang, J., Anderson, C.E., Schilling, J.S., 2018. Oxidative damage control during decay of wood by Brown rot fungus using oxygen radicals. Appl. Environ. Microbiol. 84 https://doi.org/10.1128/AEM.01937-18 e01937-18,/aem/84/22/e01937-18.atom.

CEN, 2020a. EN 113-1. Durability of Wood and Wood-Based Products. Test Method against Wood Destroying Basidiomycetes. Part 1: Assessment of Biocidal Efficacy of Wood Preservatives. European Committee for Standardization, Brussels, Belgium.

CEN, 2020b. EN 113-2. Durability of Wood and Wood-Based Products. Test Method against Wood Destroying Basidiomycetes. Part 2: Assessment of Inherent or Enhanced Durability. European Committee for Standardization, Brussels, Belgium.

Curran, P.J., 1989. Remote sensing of foliar chemistry. Remote Sens. Environ. 30, 271–278. https://doi.org/10.1016/0034-4257(89)90069-2.

de Jong, S., 1993. SIMPLS: an alternative approach to partial least squares regression. Chemometr. Intell. Lab. Syst. 18, 251–263. https://doi.org/10.1016/0169-7439(93)85002-X.

Fackler, K., Schwanninger, M., 2012. How spectroscopy and microspectroscopy of degraded wood contribute to understand fungal wood decay. Appl. Microbiol. Biotechnol. 96, 587–599. https://doi.org/10.1007/s00253-012-4369-5.

Fackler, K., Schwanninger, M., 2010. Polysaccharide degradation and lignin modification during Brown rot of spruce wood: a polarised fourier transform near infrared study. J. Near Infrared Spectrosc. 18, 403–416. https://doi.org/10.1255/jnirs.901.

Fackler, K., Schwanninger, M., Gradinger, C., Hinterstoisser, B., Messner, K., 2007. Qualitative and quantitative changes of beech wood degraded by wood-rotting basidiomycetes monitored by Fourier transform infrared spectroscopic methods and multivariate data analysis. FEMS Microbiol. Lett. 271, 162–169. https://doi.org/10.1111/j.1574-6968.2007.00712.x.

Fernandes, A., Lousada, J., Morais, J., Xavier, J., Pereira, J., Melo-Pinto, P., 2013. Measurement of intra-ring wood density by means of imaging VIS/NIR spectroscopy (hyperspectral imaging). Holzforschung 67, 59–65. https://doi.org/10.1515/hf-2011-0258.

Flæte, P.O., Haartveit, E.Y., 2004. Non-destructive prediction of decay resistance of pinus sylvestris heartwood by near infrared spectroscopy. Scand. J. For. Res. 19, 55–63. https://doi.org/10.1080/02827580410017852.

Geladi, P., MacDougall, D., Martens, H., 1985. Linearization and scatter-correction for near-infrared reflectance spectra of meat. Appl. Spectrosc. 39, 491–500. https://doi.org/10.1366/0003702854248656.

Goodell, B., Zhu, Y., Kim, S., Kafle, K., Eastwood, D., Daniel, G., Jellison, J., Yoshida, M., Groom, L., Pingali, S.V., O'Neill, H., 2017. Modification of the nanostructure of lignocellulose cell walls via a non-enzymatic lignocellulose deconstruction system in brown rot wood-decay fungi. Biotechnol. Biofuels 10, 179. https://doi.org/10.1186/s13068-017-0865-2.

Jochemsen, A., 2022. SWIR spectra of basidiomycete decay of Scots pine. Mendeley Data V1. https://doi.org/10.17632/st7f3g6mk4.1.

Kelley, S.S., Jellison, J., Goodell, B., 2002. Use of NIR and pyrolysis-MBMS coupled with multivariate analysis for detecting the chemical changes associated with brown-rot biodegradation of spruce wood. FEMS Microbiol. Lett. 209, 107–111. https://doi.org/10.1111/j.1574-6968.2002.tb11117.x.

Kirk, T.K., Adler, E., 1970. Methoxyl-deficient structural elements in lignin of sweetgum decayed by a brown-rot fungus. Acta Chem. Scand. 24, 3379–3390.

Kobori, H., Gorretta, N., Rabatel, G., Bellon-Maurel, V., Chaix, G., Roger, J.-M., Tsuchikawa, S., 2013. Applicability of Vis-NIR hyperspectral imaging for monitoring wood moisture content (MC). Holzforschung 67, 307–314. https://doi.org/10.1515/hf-2012-0054.

Kokaly, R.F., Clark, R.N., Swayze, G.A., Livo, K.E., Hoefen, T.M., Pearson, N.C., Wise, R. A., Benzel, W.M., Lowers, H.A., Driscoll, R.L., Klein, A.J., 2017. USGS Spectral Library Version 7 (Report No. 1035), Data Series. https://doi.org/10.3133/ds1035. Reston, vol. A.

Korripally, P., Timokhin, V.I., Houtman, C.J., Mozuch, M.D., Hammel, K.E., 2013. Evidence from Serpula lacrymans that 2,5-dimethoxyhydroquinone is a lignocellulolytic agent of divergent Brown rot basidiomycetes. Appl. Environ. Microbiol. 79, 2377–2383. https://doi.org/10.1128/AEM.03880-12.

Lestander, T., Geladi, P., Larsson, S., Thyrel, M., 2012. Near infrared image analysis for online identification and separation of wood chips with elevated levels of extractives. J. Near Infrared Spectrosc. 20, 591. https://doi.org/10.1255/jnirs.992.

Martens, H., Nielsen, J.P., Engelsen, S.B., 2003. Light scattering and light absorbance separated by extended multiplicative signal correction. Application to near-infrared transmission analysis of powder mixtures. Anal. Chem. 75, 394–404. https://doi.org/10.1021/ac020194w.

Martens, H., Stark, E., 1991. Extended multiplicative signal correction and spectral interference subtraction: new preprocessing methods for near infrared spectroscopy. J. Pharm. Biomed. Anal. 9, 625–635. https://doi.org/10.1016/0731-7085(91)80188-F.

Otjen, L., Blanchette, R., 1987. Assessment of 30 White Rot Basidiomycetes for Selective Lignin Degradation, vol. 41, p. 7.

Ozaki, Y., Huck, C., Tsuchikawa, S., Engelsen, S.B., 2021. Near-Infrared Spectroscopy. Springer Singapore, S.l.

Presley, G.N., Panisko, E., Purvine, S.O., Schilling, J.S., 2018. Coupling secretomics with enzyme activities to compare the temporal processes of wood metabolism among white and Brown rot fungi. Appl. Environ. Microbiol. 84 https://doi.org/10.1128/AEM.00159-18 e00159-18,/aem/84/16/e00159-18.atom.

Presley, G.N., Schilling, J.S., 2017. Distinct growth and secretome strategies for two taxonomically divergent Brown rot fungi. Appl. Environ. Microbiol. 83 (-16), e02987 https://doi.org/10.1128/AEM.02987-16 e02987-16.

Presley, G.N., Zhang, J., Purvine, S.O., Schilling, J.S., 2020. Functional genomics, transcriptomics, and proteomics reveal distinct combat strategies between lineages of wood-degrading fungi with redundant wood decay mechanisms. Front. Microbiol. 11, 1646. https://doi.org/10.3389/fmicb.2020.01646.

Riley, R., Salamov, A.A., Brown, D.W., Nagy, L.G., Floudas, D., Held, B.W., Levasseur, A., Lombard, V., Morin, E., Otillar, R., Lindquist, E.A., Sun, H., LaButti, K.M., Schmutz, J., Jabbour, D., Luo, H., Baker, S.E., Pisabarro, A.G., Walton, J.D., Blanchette, R.A., Henrissat, B., Martin, F., Cullen, D., Hibbett, D.S., Grigoriev, I.V., 2014. Extensive sampling of basidiomycete genomes demonstrates inadequacy of the white-rot/brown-rot paradigm for wood decay fungi. Proc. Natl. Acad. Sci. USA 111, 9923–9928. https://doi.org/10.1073/pnas.1400592111.

Rowell, R.M. (Ed.), 2005. Handbook of Wood Chemistry and Wood Composites. CRC Press, Boca Raton, Fla.

Russell, T., Anderson, P., 2017. The Illustrated Encyclopedia of Trees of Britain and Europe: the Ultimate Reference Guide and Identifier to 550 of the Most Spectacular, Best-Loved and Unusual Trees, with 1600 Specially Co. Anness Publishing.

Sandak, A., Ferrari, S., Sandak, J., Allegretti, O., Terziev, N., Riggio, M., 2013. Monitoring of wood decay by near infrared spectroscopy. Adv. Mater. Res. 778, 802–809. https://doi.org/10.4028/www.scientific.net/AMR.778.802.

Sandak, A., Sandak, J., Riggio, M., 2016. Assessment of wood structural members degradation by means of infrared spectroscopy: an overview: assessment of Wood Degradation by Means of Spectroscopy. Struct. Control Health Monit. 23, 396–408. https://doi.org/10.1002/stc.1777.

Sandak, J., Sandak, A., Meder, R., 2016. Assessing trees, wood and derived products with near infrared spectroscopy: hints and tips. J. Near Infrared Spectrosc. 24, 485–505. https://doi.org/10.1255/jnirs.1255.

Sandak, J., Sandak, A., Zitek, A., Hintestoisser, B., Picchi, G., 2020. Development of low-cost portable spectrometers for detection of wood defects. Sensors 20, 545. https://doi.org/10.3390/s20020545.

Schilling, J.S., Ai, J., Blanchette, R.A., Duncan, S.M., Filley, T.R., Tschirner, U.W., 2012. Lignocellulose modifications by brown rot fungi and their effects, as pretreatments, on cellulolysis. Bioresour. Technol. 116, 147–154. https://doi.org/10.1016/j.biortech.2012.04.018.

Schwanninger, M., Hinterstoisser, B., Gradinger, C., Messner, K., Fackler, K., 2004. Examination of spruce wood biodegraded by ceriporiopsis subvermispora using near and mid infrared spectroscopy. J. Near Infrared Spectrosc. 12, 397–409. https://doi.org/10.1255/jnirs.449.

Schwanninger, M., Rodrigues, J.C., Fackler, K., 2011. A review of band Assignments in near infrared spectra of wood and wood components. J. Near Infrared Spectrosc. 19, 287–308. https://doi.org/10.1255/jnirs.955.

Seifert, K.A., 1983. Decay. Of wood by the dacrymycetales. Mycologia 75, 1011–1018. https://doi.org/10.1080/00275514.1983.12023787.

Sjöström, E., 1993. Wood Chemistry: Fundamentals and Applications, second ed. Academic Press, San Diego.

Smeland, K.A., Liland, K.H., Sandak, J., Sandak, A., Gobakken, L.R., Thiis, T.K., Burud, I., 2016. Near infrared hyperspectral imaging in transmission mode: assessing the weathering of thin wood samples. J. Near Infrared Spectrosc. 24, 595–604. https://doi.org/10.1255/jnirs.1253.

Stefansson, P., Thiis, T., Gobakken, L.R., Burud, I., 2020. Hyperspectral NIR time series imaging used as a new method for estimating the moisture content dynamics of thermally modified Scots pine. Wood Mater. Sci. Eng. 1–9. https://doi.org/10.1080/17480272.2020.1772366.

Toivanen, T.-J., Alén, R., 2006. Variations in the chemical composition within pine (Pinus sylvestris) trunks determined by diffuse reflectance infrared spectroscopy and chemometrics. Cellulose 13, 53–61. https://doi.org/10.1007/s10570-005-9016-1.

Tsuchikawa, S., 2007. A review of recent near infrared research for wood and paper. Appl. Spectrosc. Rev. 42, 43–71. https://doi.org/10.1080/05704920601036707.

Tsuchikawa, S., Kobori, H., 2015. A review of recent application of near infrared spectroscopy to wood science and technology. J. Wood Sci. 61, 213–220. https://doi.org/10.1007/s10086-015-1467-x.

Tsuchikawa, S., Schwanninger, M., 2013. A review of recent near-infrared research for wood and paper (Part 2). Appl. Spectrosc. Rev. 48, 560–587. https://doi.org/10.1080/05704928.2011.621079.

Umezawa, K., Niikura, M., Kojima, Y., Goodell, B., Yoshida, M., 2020. Transcriptome analysis of the brown rot fungus Gloeophyllum trabeum during lignocellulose degradation. PLoS One 15, e0243984. https://doi.org/10.1371/journal.pone.0243984.

Wei, D., Houtman, C.J., Kapich, A.N., Hunt, C.G., Cullen, D., Hammel, K.E., 2010. Laccase and its role in production of extracellular reactive oxygen species during wood decay by the Brown rot basidiomycete postia placenta. Appl. Environ. Microbiol. 76, 2091–2097. https://doi.org/10.1128/AEM.02929-09.

Winandy, J.E., Morrell, J.J., 1993. Relationship between incipient decay, strength, and chemical composition of Douglas-fir heartwood. Wood Fiber Sci. 278–288.

Witomski, P., Olek, W., Bonarski, J.T., 2016. Changes in strength of Scots pine wood (Pinus silvestris L.) decayed by brown rot (Coniophora puteana) and white rot (Trametes versicolor). Construct. Build. Mater. 102, 162–166. https://doi.org/10.1016/j.conbuildmat.2015.10.109.

Wu, B., Gaskell, J., Held, B.W., Toapanta, C., Vuong, T., Ahrendt, S., Lipzen, A., Zhang, J., Schilling, J.S., Master, E., Grigoriev, I.V., Blanchette, R.A., Cullen, D., Hibbett, D.S., 2018. Substrate-specific differential gene expression and RNA editing in the Brown rot fungus *Fomitopsis pinicola*. Appl. Environ. Microbiol. 84 https://doi.org/10.1128/AEM.00991-18 e00991-18,/aem/84/16/e00991-18.atom.

Yelle, D.J., Ralph, J., Lu, F., Hammel, K.E., 2008. Evidence for cleavage of lignin by a brown rot basidiomycete. Environ. Microbiol. 10, 1844–1849. https://doi.org/10.1111/j.1462-2920.2008.01605.x.

Yelle, D.J., Wei, D., Ralph, J., Hammel, K.E., 2011. Multidimensional NMR analysis reveals truncated lignin structures in wood decayed by the brown rot basidiomycete Postia placenta: ligninolysis during fungal brown rot of wood. Environ. Microbiol. 13, 1091–1100. https://doi.org/10.1111/j.1462-2920.2010.02417.x.

Zabel, R.A., Morrell, J.J., 2020. Wood Microbiology: Decay and its Prevention. Academic Press.

Zelinka, S.L., Jakes, J.E., Kirker, G.T., Bishell, A.B., Boardman, C.R., Lai, B., Sterbinsky, G.E., Jellison, J., Goodell, B., 2021. Oxidation states of iron and manganese in lignocellulose altered by the brown rot fungus Gloeophyllum trabeum measured in-situ using X-ray absorption near edge spectroscopy (XANES). Int. Biodeterior. Biodegrad. 158, 105162 https://doi.org/10.1016/j.ibiod.2020.105162.

Zhang, J., Hu, D., Orr, G., Schilling, J., 2019a. Fluorescence in situ mRNA hybridization for gene expression detection in a wood decay fungus. Int. Biodeterior. Biodegrad. 143, 104731 https://doi.org/10.1016/j.ibiod.2019.104731.

Zhang, J., Mitchell, H.D., Markillie, L.M., Gaffrey, M.J., Orr, G., Schilling, J., 2019b. Reference genes for accurate normalization of gene expression in wood-decomposing fungi. Fungal Genet. Biol. 123, 33–40. https://doi.org/10.1016/j.fgb.2018.11.005.

Zhang, J., Presley, G.N., Hammel, K.E., Ryu, J.-S., Menke, J.R., Figueroa, M., Hu, D., Orr, G., Schilling, J.S., 2016. Localizing gene regulation reveals a staggered wood decay mechanism for the brown rot fungus *Postia placenta*. Proc. Natl. Acad. Sci. USA 113, 10968–10973. https://doi.org/10.1073/pnas.1608454113.

Zhang, J., Schilling, J.S., 2017. Role of carbon source in the shift from oxidative to hydrolytic wood decomposition by Postia placenta. Fungal Genet. Biol. 106, 1–8. https://doi.org/10.1016/j.fgb.2017.06.003.

Zhang, J., Silverstein, K.A.T., Castaño, J.D., Figueroa, M., Schilling, J.S., 2019c. Gene regulation shifts shed light on fungal adaption. Plant Biomass Decomposers 10, 15.

Zhu, Y., Plaza, N., Kojima, Y., Yoshida, M., Zhang, J., Jellison, J., Pingali, S.V., O'Neill, H., Goodell, B., 2020. Nanostructural analysis of enzymatic and non-enzymatic Brown rot fungal deconstruction of the lignocellulose cell wall. Front. Microbiol. 11, 1389. https://doi.org/10.3389/fmicb.2020.01389.